Conference Paper, Published Version

Roeber, Volker; Pinault, Jonas; Morichon, Denis; Abadie, Stephane; Azouri, Assaf; Guiles, Martin; Luther, Doug; Delpey, Matthias; Danglade, Nikola

Improving Wave Run-up Forecasts – Benefits from Phase-resolving Models

Coastal Structures 2019 - Nils Goseberg, Torsten Schlurmann (eds) - © 2019 Bundesanstalt für Wasserbau
ISBN 978-3-939230-64-9 (Online) - DOI: 10.18451/978-3-939230-64-9_075

Improving Wave Run-up Forecasts – Benefits from Phase-resolving Models

V. Roeber[1,2], J. Pinault[1], D. Morichon[1], S. Abadie[1],
A. Azouri[2], M. Guiles[2], D. S. Luther[2],
M. Delpey[3], N. Danglade[3]

[1]*Université de Pau et des Pays de l'Adour, E2S UPPA, Chaire HPC-Waves, Laboratoire SIAME, Anglet, France*

[2]*University of Hawai'i at Mānoa, Department of Oceanography, Honolulu, Hawai'i, USA*

[3]*Rivages Pro Tech, SUEZ Eau France, Bidart, France*

Abstract: Accurate wave run-up forecasting is essential for coastal zone management, hazard prevention, and assessment of damage potentials to coastal infrastructure. Most wave forecasting tools are based on numerical solutions of the spectral wave action balance equation that provide an estimate of the evolution of the wave spectrum but neither describe the propagation of individual waves in the surf zone nor wave run-up on land. Pragmatically, wave run-up forecasts have been utilizing empirical formulations that act as transfer functions between offshore wave conditions and run-up. Observations and modeling work around Hawaii and along the French Basque coast have shown that wave run-up processes can locally be highly variable. The response of the coastline and the subsequent local run-up is generally dominated by a combination of gravity and infra-gravity motions with the latter involving modes ranging in periods from 1 minute to nearly 30 minutes. Solutions from depth-integrated wave models - such as of non-hydrostatic and Boussinesq-type - carry the potential to offer a more accurate and complete description of the coastal wave processes including infra-gravity waves and run-up/inundation over large areas and should be considered for inclusion in operational wave run-up forecasts.

Keywords: Nearshore waves, depth-integrated model, Boussinesq, non-hydrostatic, wave run-up, forecast

1 Introduction

Large open ocean swell waves impinging on distant shorelines frequently result in coastal flooding, hazardous currents, infrastructure damage, and erosion. In combination with high water levels, such as during spring tides, these energetic swells result in much more than "nuisance flooding". With the anticipated rise in global sea level, the present problems will likely intensify in the future and pose serious problems to coastal communities.

1.1 Operational wave run-up forecast

To prepare for potential hazards, researchers from the Pacific Islands Ocean Observing System (PacIOOS) have developed and implemented real-time forecasts of coastal flooding driven by remotely generated swell waves (e.g. Guiles et al., 2019). Though these forecasts[1] are not intended to replace warnings from official emergency management personnel, they have proven precious to coastal managers and property owners for responding to short-term threats to lives and property in Hawai'i and also in the Republic of the Marshall Islands (Hess et al., 2015). The forecast relies on the general wave field computed by NOAA's WAVEWATCH III (WW3; Tolman, 2009) model. The spectral output at several virtual buoy locations offshore from the coast provides a 7-day swell

[1]http://www.pacioos.hawaii.edu/shoreline-category/runup/

forecast on a real-time basis. Since WW3 solves the spectral wave action balance equation, it is computing the spectral density function that tells how much of the waves' free surface elevation variance is contained in particular bins of frequencies and directions. The main assumption behind the governing equations of spectral wave models is that time and space scales of the variation of the wave field, water depth, and currents are much larger than the variation scales of a single wave in the system. The solution of the overall wave statistics of the wave field instead of the free surface directly allows for computation of the wave energy propagation over global scales at relatively low computational cost. The output from such wave models is therefore similar to the data provided by wave buoys, which derive directional wave spectra from the recorded time series at pressure sensors or directly from the buoys' motion. In the case of the PacIOOS forecast for the Northshore of O'ahu, Hawai'i, observations from the PacIOOS Waimea Buoy (CDIP106) serve for quality control purposes of the WW3 spectra in 200 m water depth.

The aforementioned 7-day swell forecast in combination with tidal and longer-period sea level forecasts provide the localized prediction in the coastal vicinity. These swell and sea level forecasts are the main input components to the empirical wave run-up model based on the model of Stockdon et al. (2006) and calibrated with nearshore data (e.g., Merrifield et al., 2014). The run-up forecast is essentially projecting the general wave statistics from water depths of around 200 m to an elevation on shore in form of a transfer function. Empirical run-up estimations such as the one developed by Stockdon et al. (2006) take care of the entire wave transformation processes including wave breaking. The forecast has proven its overall validity in numerous events despite its rather general assumptions and simplicity.

2 Phase-resolving wave models

Future scenarios of global wave activities and sea level rise urge scientists and coastal zone managers to increase their efforts toward more accurate and also refined forecasting of wave-driven run-up and flooding. Coverage for these types of hazards is an ongoing effort with a forecasting system under development along the coastline of West Maui, Hawai'i, and along the Côte Basque in SW France. The objective in the future is the operation of an advanced notification system for coastal communities of hazards arising from swell waves. These predictions will be based on computations from phase-resolving numerical models, which to date are not commonly utilized for wave run-up and inundation forecasts.

2.1 Phase-resolving vs. phase-averaged

The underlying concept of phase-resolving numerical wave models is based on the consideration of time and space scales of single waves, which implies that the overall wave field is the result from the superposition of multiple individual waves. With the distribution of sea surface elevation around the mean water level (zero-crossing), the free surface evolution is directly affected by the local variations in bathymetry, wave-wave interactions, and wave breaking. These processes require high spatial resolution; therefore phase-resolving models typically use a much finer mesh than phase-averaged models. Due to the associated computational constraints, the model domains usually cover areas on the order of several square kilometers in contrast to square degrees. Of course, this is different in the case of tsunami computations where the spatial scale of individual waves spans over several kilometers, therein allowing for the use of much coarser numerical meshes.

An advantage of phase-resolving models is that they inherently compute second-order effects such as wave set-up, recirculation, and infra-gravity waves as a result of the free surface evolution without the need for parameterized conditions. With an appropriate treatment of flow discontinuities, as it is necessary for breaking waves, these models can compute energy dissipation and momentum transfer directly for an individual wave or equally an envelope of multiple waves. Variations of incoming wave groups automatically result in temporal fluctuations of the wave set-up (surf beat), which can vary locally.

In contrast, phase-averaged models require parameterization of some processes including the wave breaking probability and the subsequent dissipation rate. In shallow water, a breaker index usually limits the wave height to a fraction of the local water depth. Since no free surface is resolved in phase-

averaged models, features like wave run-up or infra-gravity motions such as surf beat cannot be computed by the governing equations. The transfer of energy from gravity to infra-gravity bands is a field of active development, since the present phase-averaged models do not account for it. This is probably the biggest limitation of phase-averaged models to nearshore wave and run-up scenarios where bound and free infra-gravity waves play an important role.

To circumvent this limitation and to still be able to obtain meaningful run-up estimates, empirical relations derived from large sets of field data (e.g. Stockdon, 2006) can be used to close the gap between run-up and offshore wave conditions. This is the approach of the existing PacIOOS forecast described in 1.1.

2.2 Non-hydrostatic vs. Boussinesq-type models

A number of phase-resolving models have been developed over the past years. *COULWAVE* (Lynett et al., 2002), *FUNWAVE* (Shi et al., 2012), *XBeach* (Roelvink et al., 2009) and *BOSZ* (Boussinesq Ocean and Surf Zone model; Roeber & Cheung, 2012a) are among those that have been extensively validated with laboratory data and also successfully used for real-world applications. The latter was chosen for the development and implementation of our forecasts.

Boussinesq-type and non-hydrostatic equations have become popular over the past 20-30 years due to increased computing power and advances in the theoretical formulations, which have lead to governing equations of relatively simple – yet powerful – form. Though there are particular differences with respect to the derivation between non-hydrostatic and Boussinesq-type equations, there are in fact more commonalities than discrepancies in the two techniques regarding their applicability and limitations.

Many non-hydrostatic equations were inspired by the concepts presented by Casulli & Stelling (1998). The governing equations are derived in a similar way as the Nonlinear Shallow Water Equations with the difference that the vertical momentum equation is retained in the form of a linear relation of the vertical velocity over depth. This gives rise to a first-order estimate of non-hydrostatic effects, which allows for pressure correction under weakly dispersive waves. More modern approaches utilize multiple layers to better approximate the vertical variation in pressure; however at significantly higher computation cost.

Though the basic concepts were introduced by Boussinesq (1871), the modern form of Boussinesq-type equations gained popularity through the seminal work of Peregrine (1967). However, the use of this type of equations in computer models only gained popularity at a later stage when Madsen & Soerensen (1992) and Nwogu (1993) presented two sets of equations derived from different concepts but with identical nonlinear and non-hydrostatic properties. As an example, the equations from Nwogu (1993) arise from the Euler equations of motion based on the assumptions of low amplitude waves in relatively shallow water ($kh < \pi$). Depth integration in combination with boundary conditions expresses the vertical velocity and pressure in form of gradients of the horizontal velocities. Though the vertical velocity varies linearly over depth - as it is the case in the aforementioned non-hydrostatic equations, substitution of the vertical velocity into a Taylor series expansion of the horizontal velocities provides a quadratic variation of the pressure and horizontal velocity profile over depth. Boussinesq-type equations account for non-hydrostatic effects through additional terms in the horizontal momentum equations and do not retain the vertical momentum equation. The dispersion properties are generally superior to one-layer non-hydrostatic models.

Both approaches reduce to the Nonlinear Shallow Water Equation after omitting the non-hydrostatic pressure corrections. Since the dispersion is a rather low-order estimate, both types of equations require shallow to intermediate water depths to ensure their validity, i.e. the wavelengths should ideally be longer than twice the local water depth ($kh < \pi$). The equations can obviously provide converging solutions for waves shorter than this threshold with the consequence that the error in phase speed increases. Though Boussinesq-type equations can handle shorter waves than the conventional one-layer non-hydrostatic equations, both methods were derived on similar physical assumptions, i.e. the range of applicability and also many numerical challenges are similar.

One of the common difficulties with respect to numerical solutions arises from wave breaking. Depth-integrated models cannot describe overturning waves, since no vertical array of cells is available. The closest to an overturning wave the solution can reach is a vertical step. However, the parabolic properties of the dispersive terms do not per se allow for discontinuities. A common work-around is the local elimination of non-hydrostatic pressure terms around the wave face to let the

hyperbolic structure of the underlying shallow water equations handle the propagation of breaking waves as shocks or bores. With the local acceleration terms expressed in conserved variables, momentum is conserved throughout the shock and the breaking waves travel with the correct height and speed.

Another challenge of these models is the presence of a Poisson-type system of equations as a result of the space-time-dependent variables. While the non-hydrostatic equations require an iterative solution of an *xy*-dependent system of equations, the Boussinesq-type equations give rise to only a sequence of one-dimensional problems with data dependency in either the *x*-direction or the *y*-direction. This is of advantage with respect to the implementation of the code in a parallel computer structure.

3 Best-Practices for the use of phase-resolving wave models

With the objective to improve a run-up forecast, phase-resolving models are expected to perform well in the vicinity of the shoreline. This includes correct representation of the water level (wave setup), infragravity wave patterns, and run-up of individual waves. The run-up itself is a challenging feature for numerical models because of the dynamically moving wet/dry boundary.

3.1 Wave generation

It is important to understand the limitations of numerical models so that they are used correctly and to their best potential for wave fore- and hindcasting. A basic source or errors results from the approximate nature of the underlying governing equations. Here, we use the equations by Nwogu (1993) as an example. Like most Boussinesq-type equations, Nwogu's (1993) formulation leads to a positive error in phase speed for $kh > \pi$ with the consequence that wavelength and celerity are over-estimated in comparison to Airy wave theory. To avoid unnecessary problems from the beginning of the computation, it is important to only generate the waves that the model can properly handle. It is a common approach in phase-resolving models to generate the input waves in the form of a wave spectrum through superposition of individual monochromatic waves such as presented in Wei et al. (1999).

Linear wave theory shows a clear dependence of the wavelength on the local water depth. The longer the wavelength, the earlier it is affected by the water depth. Fig. 1 shows the error between the equation by Nwogu (1993) (thin blue lines) and Airy wave theory (thick dashed black lines) for various water depths. With increasing water depth a wave with a particular period is subject to larger errors in celerity and length. It is therefore important to ensure compatibility between the water depth at the wavemaker and the frequencies of the input spectrum. In some cases it is necessary to truncate the high frequency tail of the input spectrum.

As an example, we look at the thin, dotted gray lines, which indicate the wavelengths of an 8 sec wave in different water depths. Linear wave theory shows that a wave of 8 sec period will be of almost 100 m length in water deeper than 50 m. In 25 m water depth, the wave will be slightly shorter. With Nwogu's (1993) Boussinesq-type approximation however, the 8 sec wave will be computed at a length of about 105 m in 50 m water depth and even of 123 m length in water of 100 m depth. This corresponds to the progressing errors between $kh = \pi$ and $kh = 2\pi$. To avoid excessively large errors in phase speed, input wave spectra should be truncated between $kh = \pi$ and $kh = 2\pi$ depending on the amount of energy in the high frequencies. The green and red lines mark these limits for each of the selected water depths respectively.

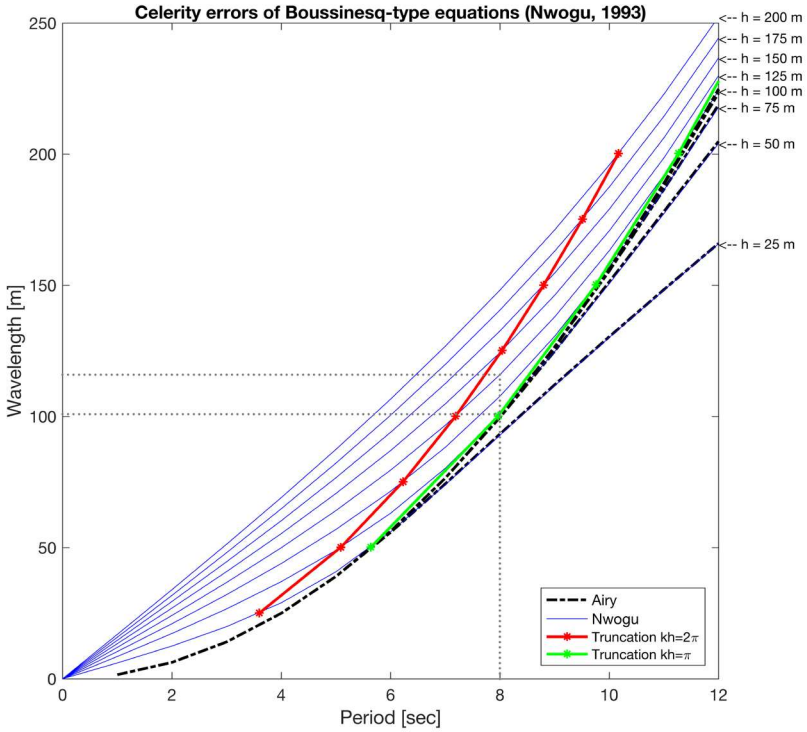

Fig. 1. Wavelength for the linearized Nwogu (1993) equation (with the flow velocities evaluated at a reference depth $z_{\alpha} = -0.55502h$) in comparison to Airy wave theory for selected water depths (h). The gray, dotted lines denote the wave lengths for a wave with 8 sec period in 50 m and 100 m water depth corresponding to $kh = \pi$ ($L/h = 2$, green line) and $kh = 2\pi$ ($L/h = 1$, red line). Difference between red and green line is associated to the error in the dispersion approximation.

Like in this example, a spectrum truncated at $kh = \pi$ with an offshore water depth of 50 m will include wave periods longer than 8 sec. Shorter waves are considered as the "high-frequency" tail and cropped. The energy from the tail can be redistributed over the remaining spectrum to ensure conservation of total energy, i.e. the significant wave height will not change. If the offshore water depth was 100 m and again $kh = \pi$ was chosen as threshold, then the shortest wave period would be of about 11 sec period. Alternatively, the spectrum could be truncated at $kh = 2\pi$, which would lead to a shortest input wave of about 7 sec, however the short waves would carry a larger error in phase speed.

It is well understood that waves are subject to the dispersion relation, which causes longer waves to travel faster than shorter waves leading to momentary superposition of multiple single waves. This is known as wave grouping. A distribution of frequencies of little variation will result in long intervals of wave groups. Longuet-Higgins (1984) found that the distribution of energy in the spectrum can give information about the minimum time required for wave groups to occur. Though wave groups are all of different magnitude and length, a general tendency can be derived from the three lowest moments in the spectrum as

$$T_{group} = \sqrt{2\pi e \frac{\mu_0}{\mu_2}}, \quad \text{with } \mu_0 = m_0 \text{ and } \mu_2 = m_2 - m_1^2/m_0, \quad m_{0,1,2} = 0^{th},\ 1^{st},\ 2^{nd} \text{ moment} \tag{1}$$

It becomes evident that excessive truncation of the high-frequency tail of the spectrum can greatly distort the bound wave components of the resulting wave field and subsequently the magnitudes and periods of local infra-gravity modes – all of which can impact the wave run-up. The truncation of the input wave spectrum always leads to an increase in the wave group period, T_{group}. To avoid drastic changes in the composition of the spectrum, it is generally recommended to move the wavemaker closer to shore (into shallower water) than to excessively truncate the tail of the wave spectrum.

3.2 Computed time

Another important factor for a successful computation of swell waves from phase-resolving models is the total computed time, i.e. the length of the model run (not to be confused with computation time, which is the time it takes a computer to complete the model run). It is trivial that the wave field needs some time to evolve, since the computation is starting from quiescent conditions. The computation

should also then be long enough to generate a statistically reasonable number of long infragravity band oscillations. It is somewhat unclear how long the computation has to be to provide the maximum wave height possible in a certain swell window, since this value is highly dependent on depth and local wave transformation. Some guidelines can be found in Montoya & Lynett (2018).

Care should be taken in terms of wave group artifacts through recycling of the input time series. Often, the wave input for phase-resolving models comes from spectra generated by phase-averaged models or wave buoys. These spectra have typically bi-linearly or logarithmically spaced frequency increments. However, the smallest frequency bin is often on the order of 0.005 Hz. Using this example, the resulting time series of the free surface elevation would recycle once every 200 sec, which is a typical infra-gravity oscillation mode or harbor resonance frequency. The inverse of the frequency increment, $1/\Delta f$, dictates the time it takes for all individual waves to interact with each other. If one wanted to eliminate the possibility of wave input recycling, one would have to adjust the frequency spacing so that $\Delta f < 1/T_{comp}$ (with T_{comp} denoting the total computed time). This will require interpolating the input spectrum to much finer resolution than usually provided - consequently, the load on the wavemaker routine increases.

3.3 Validation of local refraction processes

Many operational phase-resolving models such as Xbeach, FUNWAVE, and *BOSZ* have been extensively validated in the past (e.g. see Roeber and Cheung, 2012b). Here we include a test case for the *BOSZ* model that serves for validation of 2D wave focusing. The scenario was computed with other Boussinesq-type models in the past (e.g. Wei and Kirby, 1995, Tonelli and Petti, 2009). The test by Berkhoff et al. (1982) examines the refraction and shoaling processes of monochromatic waves over a complex 2D bathymetry. The experimental layout is shown in Fig. 2.

The input wave is monochromatic and unidirectional with a period of $T = 1$ s and an amplitude of $A = 0.0232$ m corresponding to $kh \sim 0.6\pi$ at the wavemaker where the water depth is 0.45 m. The numerical domain is composed of quadratic cells of 0.05 m length, solid reflective sidewalls, and sponge layers along the lower and upper ends. The wavemaker is placed away from the lower boundary of the domain to allow for the sponge layer to absorb the outgoing waves. The Courant number in *BOSZ* was set to 0.5 and the solution was obtained with a second order Runge-Kutta time integration scheme for 50 sec. The free surface elevation was recorded at 20 Hz sampling rate. The output was then analyzed by a zero-up-crossing method over the last 20 sec to obtain the mean wave heights along the six transects shown in Fig. 2.

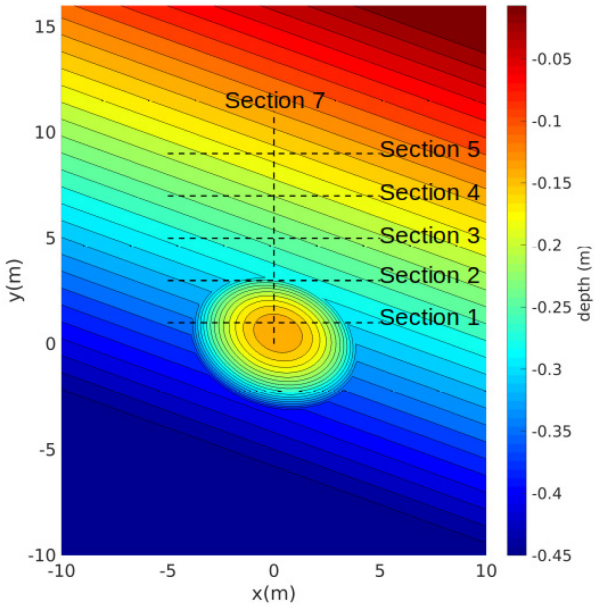

Fig. 2. Experimental layout from Berkhoff et al., 1982. The tank was 20 m wide and 22 m long, and the bathymetry consisted of a tilted slope of 1/50. An elliptic shoal was placed on the slope, centered at (0; 0). The maximum water depth is 0.45 m at the wavemaker (lower end, y = -10 m). Measurements are available along 6 transects indicated by the dashed lines. The BOSZ model domain is composed of 0.05 m by 0.05 m grid cells with solid walls on the sides and absorbing boundaries at the upper and lower end.

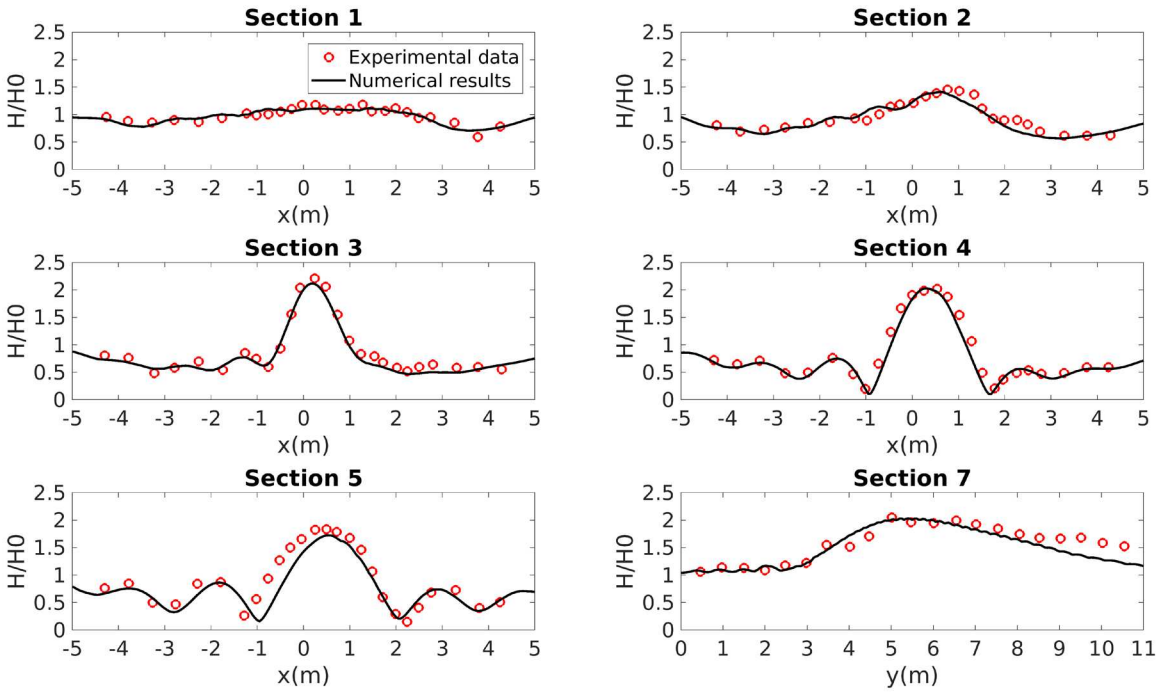

Fig. 3. Average wave heights over a range of 20 sec from the *BOSZ* model (black line) along the six transects in Fig. 2 in comparison with the experimental data (red circles) from Berkhoff et al., 1982. The input wave height was specified according to the experimental description; it was not adjusted to improve the match between model and data. Wave heights were normalized by the input signal at the wavemaker.

As the wave propagates over the slope it starts to align with the isobaths, generating an asymmetry in the profile (Fig. 3, section 1 and 2). As the shoaling process generates higher harmonics, the elliptic shoal converges the energy towards the centerline, leading to a strong but only local amplification in wave height (Fig. 3, section 3 and 4). As the waves travel away from the elliptic shoal the energy is gradually redistributed to the sides (Fig. 3, section 5). The cross-shore transect along section 7 in Fig. 3 shows the gradual increase and decrease of the height. Despite some uncertainties in the experimental layout (e.g. absorbing boundaries), the *BOSZ* model reproduces the driving processes that govern this problem without the need of excessively fine grid spacing.

4 Wave Processes around West Maui

The coastline around the western part of Maui, Hawai'i, is an example of how wave processes and energetic regimes can vary over relatively short distances as demonstrated in Azouri et al., 2019 (see Fig. 4). The coastline is a typical example for an irregular bathymetry commonly found around tropical and subtropical islands with fringing reef formations and channel systems.

The coastline around West Maui is weakly sheltered by a narrow, variable-depth fringing reef, which drops off to depths of 50-100 m about 0.5-1.0 km from shore. The model output from Fig. 4 is based on computations from the *BOSZ* model. The swell conditions describe a typical winter swell of 2 m significant wave height and 15 sec peak period from the North. The model domain was about 25 km by 15 km with 10 m by 10 m grid cells. The wave field evolved over a period of 2 hours. The wave setup, $<\eta>$, in Fig. 4 was determined along the -1 m contour from a 40-min average of the free surface time series. The gravity and infra-gravity quantities of the swell are shown for the two components in the empirical formulation of Stockdon (2006), however, with input from nearshore instead of from offshore waves.

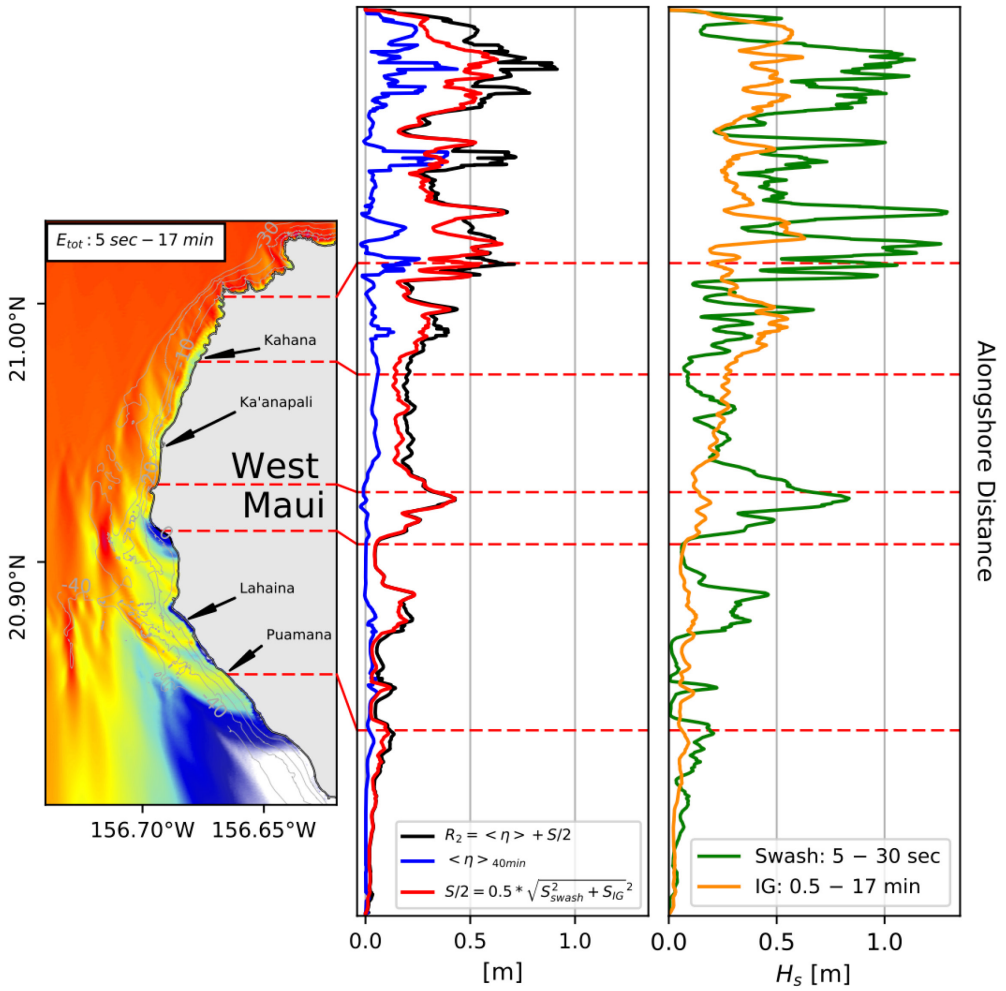

Fig. 4. North swell of H_s = 2 m and T_p = 15 sec around West Maui, Hawai'i. Left panel: total wave energy between 5 sec and 17 min period. Strong local refraction pattern are characteristic for the site. Middle panel: contributions to the 2% runup (R_2) from Stockdon (2006) in form of wave setup (<η>) and significant swash height, S. Right panel: significant wave height in the swash band (gravity waves < 30 sec) and infra-gravity (IG) band. Variables in middle and right panels are obtained at locations along the -1 m isobaths.

Noticeably, local refraction and focusing effects dominate the wave processes around the entire stretch of the coast. The reef structure locally leads to strong wave convergence with "fingers" of energy at particular locations. Even locations not facing the incoming swell direction experience high levels of energy. This is the case near Puamana (Fig. 5 shows a snapshot of the free surface elevation). Due to the fact that the total energy in the system has to be preserved, divergence effects result in some areas being protected despite their exposure to the incoming swell (e.g. Ka'anapali).

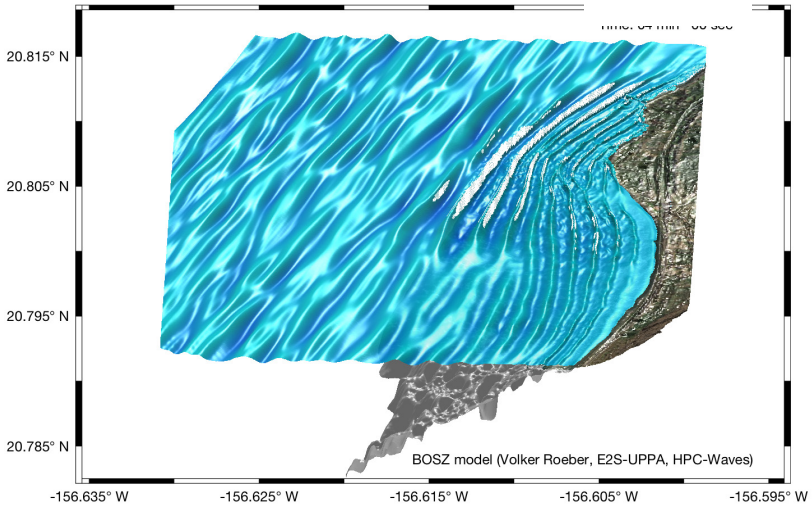

Fig. 5. Snapshot of free surface elevation from *BOSZ* at Puamana (see left panel in Fig. 4 for location) as an example of how phase-resolving models can handle complex problems of multi-directional waves over irregular bathymetry including wave breaking and run-up.

Counter-intuitively, the infra-gravity wave energy locally exceeds the energy carried in the gravity swell band (Kahana) despite the site's exposure to the approaching swell. Though computations of extreme wave scenarios had lead to similar conclusions (e.g. Roeber and Bricker, 2015), the variation of wave energy under regular swell forcing might still be somewhat unexpected. This underlines the importance of considering alongshore variability and spatial distributions of wave energy for the assessment of wave run-up. Especially, the two-dimensionality of infra-gravity wave processes, which can lead to wave run-up at far distances from their generation sites, has to be taken into account in modern hazard mitigation strategies. Empirical run-up formulations based on offshore wave conditions are not able to reliably quantify these local variations.

5 Conclusions

Phase-resolving models such as *BOSZ* can help to extend and improve wave run-up forecasts. The ability of such models to compute both gravity and infra-gravity waves and their subsequent run-up on land makes them a valuable choice for inclusion in operational forecasts. The accurate computation of local wave amplification and secondary processes such as surf beat provides a powerful extension to conventional run-up forecasts at sites where longshore variability is critical and where empirical formulations exhibit limitations.

To ensure high-quality results from phase-resolving models, systematic validation of the computer code is important; however, it is not the only requirement. In addition, it is essential to be aware of the applicability and, especially, of the limitations associated with the governing equations and the particular numerical solutions. It is therefore recommended to consult an expert before implementing these models into an operational forecasting framework.

Acknowledgments

Forecast development for West Maui was supported at the University of Hawaii by the National Oceanic and Atmospheric Administration's Office for Coastal Management Regional Coastal Resilience Program Award #NA17NOS4730143, Integrated Ocean Observing System Award #NA16NOS0120024, Hawai'i Sea Grant Award #NA140AR4170071, and the Joint Institute for Marine and Atmospheric Research.

Volker Roeber acknowledges financial support from the Isite program Energy Environment Solutions (E2S), the Communauté d'Agglomération Pays Basque (CAPB) and the Communauté Région Nouvelle Aquitaine (CRNA) for the chair position HPC-Waves.

This project has received funding from the European Union's Horizon 2020 Research and Innovation Programme.

References

Azouri, A., Roeber, V., Guiles, M., Luther, D.S., 2019. Observations and Modeling of Infragravity Waves in a Complex Reef Environment. USACE Infragravity Wave Workshop: Integrating Science and Engineering Practice, January 16-17, 2019, Scripps Institute of Oceanography, La Jolla, CA, USA.

Bellafont, F., Morichon, D., Roeber, V., André, G., Abadie, S., 2018. Infragravity period oscillations in a channel harbor near a river mouth. Coastal Engineering Proceedings, [S.l.], n. 36, p. papers.8.

Berkhoff, J.C.W., Booy, N., Radder, A.C., 1982. Verification of numerical wave propagation models for simple harmonic linear water waves, Coastal Engineering 6, 255–279.

Boussinesq, J.V., 1871. Théorie générale des mouvements qui sont propagés dans un canal rectangulaire horizontal. Comptes Rendus de l'Académie des Sciences, Paris, 73:256-260.

Casulli, V., Stelling, G.S., 1998. Numerical simulation of 3D quasi-hydrostatic free-surface flows. Journal of Hydraulic Engineerin, 124, 678-686.

Guiles, M., Azouri, A., Roeber, V., Iwamoto, M.M., Langenberger, F., Luther, D.S., 2019. Forecasts of Wave-Induced Coastal Hazards in the United States Pacific Islands: Past, Present, and the Future. Front. Mar. Sci. 6:170.

Hess, D., Hwang, D., Fellenius, K., Robertson, I., Stege, M., and Chutaro, B. (2015). Homeowner's Handbook to Prepare for Natural Hazards. Majuro: University of Hawai'i Sea Grant College Program.

Madsen, P.A., Sorensen, O.R., 1992. A new form of the Boussinesq equations with improved linear dispersion characteristics. Part 2. A slowly-varying bathymetry. Coastal Engineering, 18, 183-204.
Merrifield, M. A., Becker, J. M., Ford, M., and Y. Yao, 2014). Observations and estimates of wave-driven water leveextremes at the Marshall Islands, Geophysical Research Letters, 41, 7245–7253.
Montoya, L., Lynett, P.J., 2018. Tsunami vs infragravity surge: comparison of the physical character of extreme runup. Geophysical Research Letters, 45, 12982-12990.
Nwogu, O., 1993. Alternative form of Boussinesq equations for nearshore wave propagation. J. Waterway, Port, Coastal and Ocean Engineering, 119, 618-638.
Peregrine, D.H., 1967. Long waves on a beach. Journal of Fluid Mechanics, 27, 815-827.
Roeber, V., Cheung, K.F., 2012a. Boussinesq-type model for energetic breaking waves in fringing reef environments. Coastal Engineering, 70(1), 1-20.
Roeber, V., Cheung, K.F., 2012b. Proceedings and Results of the 2011 NTHMP Model Benchmarking Workshop, 361–406 NOAA, Washington, DC, USA, http://nws.weather.gov/nthmp/documents/nthmpWorkshopProcMerged.pdf .
Roeber, V., Bricker, J.D., 2015. Destructive tsunami-like wave generated by surf beat over a coral reef during Typhoon Haiyan. Nature Communications, 6:7854 doi: 10.1038/ncomms8854.
Roelvink, D., Reniers, A., Van Dongeren, A. P., de Vries, J. V. T., McCall, R., and Lescinski, J., 2009. Modelling storm impacts on beaches, dunes and barrier islands. Coastal Engineering, 56, 1133–1152.
Shi, F., Kirby, J. T., Harris, J. C., Geiman, J. D., and Grilli, S. T., 2012. A high-order adaptive time-stepping TVD solver for Boussinesq modeling of breaking waves and coastal inundation. Ocean Model. 43, 36–51.
Stockdon, H. F., Holman, R.A., Howd, P.A., Sallenger, A.H., 2006. Empirical parameterization of setup, swash, and run-up, Coastal Engineering, 53(7), 573-588.
Tolman, H.L., 2009. User manual and system documentation of WAVEWATCH III TM version 3.14. Techn. Note MMAB Contrib. 276:220.
Tonelli, M., Petti M., 2009. Hybrid finite volume-finite difference scheme for 2dh improved Boussinesq equations. Coastal Engineering 56, 609-620.
Wei, G., Kirby, J.T., 1995. Time-dependent numerical code for extended Boussinesq equations. Journal of Waterway, Port, Coastal, and Ocean Engineering, ASCE 121, 251–261.
Wei, G., Kirby, J.T., Sinha, A., 1999. Generation of waves in Boussinesq models using a source function method. Coastal Engineering, 36, 271-299.